

High performance $\text{Al}_x\text{Ga}_{1-x}\text{N}$ -based avalanche photodiodes

Turgut Tut^{*}, Bayram Butun, Mutlu Gokkavas, Ekmel Ozbay

*Nanotechnology Research Center, Department of Physics, Department of Electrical and Electronics Engineering,
Bilkent University, Bilkent, 06800 Ankara, Turkey*

Received 31 January 2007; received in revised form 10 May 2007; accepted 13 May 2007

Available online 21 May 2007

Abstract

We report high performance solar-blind photodetectors with reproducible avalanche gain as high as 820 under ultraviolet illumination. The solar-blind photodetectors have a sharp cut-off around 276 nm. We improved the device performance by designing different epitaxial wafer structure with thinner active multiplication layer. We compare the resulting fabricated devices from these wafers in terms of dark current, photoresponse, avalanche gain performances.

© 2007 Elsevier B.V. All rights reserved.

Keywords: AlGaIn; Solar-blind; Avalanche; Schottky

1. Introduction

The recent developments in high Al-content $\text{Al}_x\text{Ga}_{1-x}\text{N}$ material growth technology made it possible to fabricate high performance solar-blind photodetectors operating in the ultraviolet (UV) spectral region with improved receiver sensitivity, low noise, low dark current density, and high speed [1–3]. AlGaIn-based Schottky, p-i-n, and MSM photodetectors with very high performances have already been demonstrated [4,5]. The UV-filtering nature of the atmospheric ozone molecules blocks the solar radiation to reach the earth's surface for wavelengths shorter than 280 nm. In this case, ultraviolet (UV) photodetectors with cut-off wavelengths around 280 nm, which are also called solar-blind detectors, can detect very weak UV signals under intense background radiation. These devices have important applications including missile plume detection, chemical/biological agent sensing, flame alarms, covert space-to-space and submarine communications,

ozone-layer monitoring, and gas detection. Due to their high responsivity (>600 A/W), high speed, high cathode gain (on the order of a million), and low dark current properties, photomultiplier tubes (PMTs) are frequently used in such applications. However, PMTs are very expensive and bulky. Besides, they require a cooling system, and they have high operation voltages in excess of 1000 V. To achieve solar-blind detection, PMTs should also be integrated with complex and expensive filters. In order to avoid these disadvantages, high performance solid-state UV photodetectors with high internal gain are needed [6]. Wide band-gap semiconductor photodetectors, such as $\text{Al}_x\text{Ga}_{1-x}\text{N}$ with $x \sim 0.4$ are ideal candidates for this purpose. These devices are intrinsically solar-blind, in which no additional filters are needed, they have low noise [7], and fast response times [8]. The lack of high internal gain has been the major limitation for the usage of AlGaIn photodetectors for applications that require high sensitivity detectors. There have been several theoretical research work that examined the avalanche effect in GaN and AlGaIn-based structures [9–11]. Experimental work on both GaN [12–18] and AlGaIn-based [4,19,20] avalanche photodiodes (APDs) were also

^{*} Corresponding author. Tel.: +90 312 290 10 17.

E-mail address: tturgut@fen.bilkent.edu.tr (T. Tut).

reported. However, reproducible high-gain in AlGaIn-based APDs is still a major limitation. In this letter, we report the realization of solar-blind AlGaIn-based avalanche photodetectors with reproducible high avalanche gain. We obtained this performance mainly by changing the device structure from our previous wafer layer design. We compared the fabricated device performances from different wafer layer designs.

2. Wafer structures and fabrication

We utilized two wafers for this study which are designed for solar-blind operation with high avalanche gain. The epitaxial wafers were grown on a 2 in. (0 0 0 1) sapphire substrate using the Aixtron 200/4 RF-S MOCVD system located at Bilkent University Nanotechnology Research Center. For the wafer I from Table 1, a thin AlN nucleation layer and a subsequent 0.5 μm thick unintentionally doped GaN mesa isolation layer was first grown. This was followed by the growth of a highly doped ($n^+ = 2 \times 10^{18} \text{ cm}^{-3}$) 0.6 μm thick GaN ohmic contact layer and a 0.2 μm thick $\text{Al}_{0.4}\text{Ga}_{0.6}\text{N}$ layer at the same doping level. The epitaxial growth of the wafer was completed with the deposition of a 0.8 μm thick undoped $\text{Al}_{0.4}\text{Ga}_{0.6}\text{N}$ active layer. The n-type doped 0.2 μm thick $\text{Al}_{0.4}\text{Ga}_{0.6}\text{N}$ layer was used as a diffusion barrier for the photocarriers generated in the GaN ohmic contact layer. The n-type doped 0.2 μm thick $\text{Al}_{0.4}\text{Ga}_{0.6}\text{N}$ layer was used as a diffusion barrier for the photocarriers generated in the GaN ohmic contact layer. Such a diffusion barrier is expected to increase the solar-blind/near-UV rejection ratio of the detector.

We grew the second wafer as follows (Table 2). First, a thin AlN nucleation layer was deposited, and then a 0.3 μm thick AlN buffer layer was deposited. Subsequently, a highly doped ($n^+ = 1.08 \times 10^{18} \text{ cm}^{-3}$) 0.3 μm thick $\text{Al}_{0.4}\text{Ga}_{0.6}\text{N}$ layer was deposited for ohmic contact, followed by a 0.2 μm thick undoped $\text{Al}_{0.4}\text{Ga}_{0.6}\text{N}$ layer for Schottky contact. We expect to see that the devices fabricated from wafer I have high UV–vis. rejection ratio and the devices fabricated from

Table 1
AlGaIn Schottky photodetector structure from wafer I

Material	Thickness	Doping (cm^{-3})
$\text{Al}_{0.4}\text{Ga}_{0.6}\text{N}$	0.8 μm	$N^- 1 \times 10^{16}$
$\text{Al}_{0.4}\text{Ga}_{0.6}\text{N}$	0.2 μm	$N^+ 2 \times 10^{18}$
GaN	0.6 μm	$N^+ 2 \times 10^{18}$
GaN	0.5 μm	u.i.d.
AlN nucleation layer	<100 nm	u.i.d.
Sapphire substrate	~ 300	–

Table 2
AlGaIn Schottky photodetector structure from wafer II

Material	Thickness	Doping (cm^{-3})
$\text{Al}_{0.4}\text{Ga}_{0.6}\text{N}$	0.2 μm	$N^- 1 \times 10^{17}$
$\text{Al}_{0.4}\text{Ga}_{0.6}\text{N}$	0.3 μm	$N^+ 1 \times 10^{18}$
AlN	0.3 μm	u.i.d.
AlN nucleation layer	<100 nm	u.i.d.
Sapphire	~ 300	–

wafer II have low dark current and high breakdown voltage.

The samples were fabricated by using a five-step microwave-compatible fabrication process in a class-100 clean room environment. The dry etching was accomplished via reactive ion etching (RIE) under CCl_2F_2 plasma, a 20 sccm gas flow rate, and 100–200 W RF power for wafers I and II. The mesa structures of the devices were formed via the RIE process, by etching all of the layers down to the sapphire layer for better mesa isolation. After the dry etch to the middle of the ohmic contact layers, Ti/Al (100/1000 \AA) contacts were deposited via thermal evaporation and left in acetone solution for the lift-off process. The samples from the first wafer were annealed at 650 $^\circ\text{C}$, and, samples from the second wafer were annealed at 700 $^\circ\text{C}$ for 60 s in a rapid thermal annealing system. Before Schottky contact deposition, surface treatment was made with HCl solution. A ~ 100 \AA thick Au metal was evaporated in order to form Au/AlGaIn Schottky contacts. Thereafter, a 200 nm thick Si_3N_4 was deposited via plasma enhanced chemical vapor deposition for passivation with a deposition rate of 140 $\text{\AA}/\text{min}$. Finally, a ~ 0.25 μm thick Ti/Au interconnect metal was deposited and lifted-off to connect the Schottky layers to the coplanar waveguide transmission line pads.

3. Measurements and results

After fabrication, the devices were characterized in terms of current–voltage, and spectral responsivity. The resulting devices had breakdown voltages higher than 50 and 60 V from wafers I and II, respectively. To obtain better isolation, we etched down to the sapphire substrate, which enabled us to obtain lower leakage current than previous fabrications. I – V measurements of the larger area devices resulted in higher leakage currents. Therefore, we chose to use the smaller area devices with 20, 40, and 60 μm diameters. Current–voltage characterization of the fabricated Schottky photodetectors was carried out by using a Keithley 6517A high resistance electrometer with low noise triax

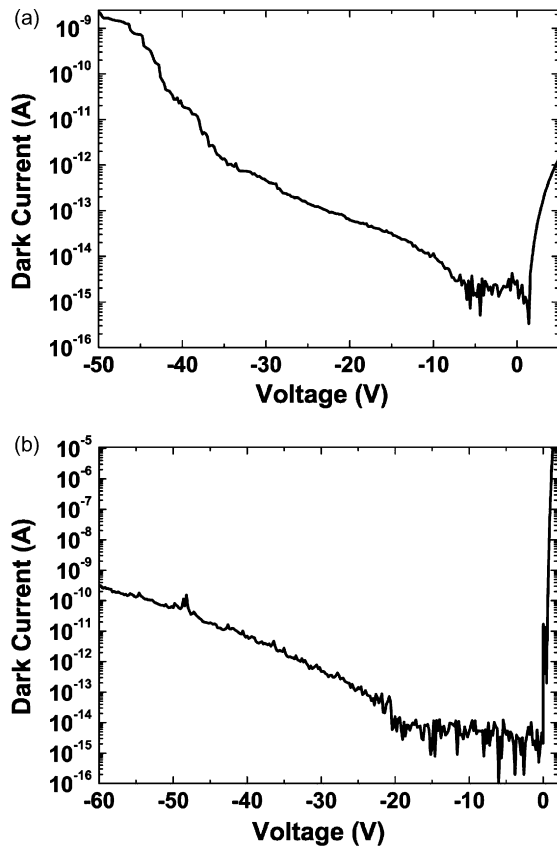


Fig. 1. Dark current results of the fabricated devices: (a) from wafer I and (b) wafer II.

cables. Fig. 1 shows the dark current of a 40 μm diameter device from the first and the second wafers, respectively. For wafer I, up to 10 V, the dark current was less than 10 fA and for wafer II up to 20 V the dark current is less than 8 fA. At 50 V bias, the device from wafer I had a dark current ~ 2 nA and from wafer II had a dark current 0.3 nA.

Fig. 2 shows the responsivity measurements of 150 μm diameter devices for different bias voltages. The peak responsivity was 0.09 A/W at a wavelength of 256 nm at 20 V reverse bias for wafer I and 0.13 A/W at a wavelength of 272 nm under the same bias voltage. The peak responsivity at the 0 V bias is 0.825 mA/W at 254 nm and 12.2 mA/W for the wafers I and II. The device had a rejection ratio of more than four orders of magnitude with wavelengths larger than 362 nm at a 20 V reverse bias for the wafer I, however, for the wafer II devices had rejection ratio three orders of magnitude with wavelength larger than 380 nm which is expected from wafer structures shown in Tables 1 and 2. Using the thermal-noise limited detectivity (D^*) formula $D^* = R_\lambda(R_0/4kT)^{1/2}$, where R_λ is the device responsivity

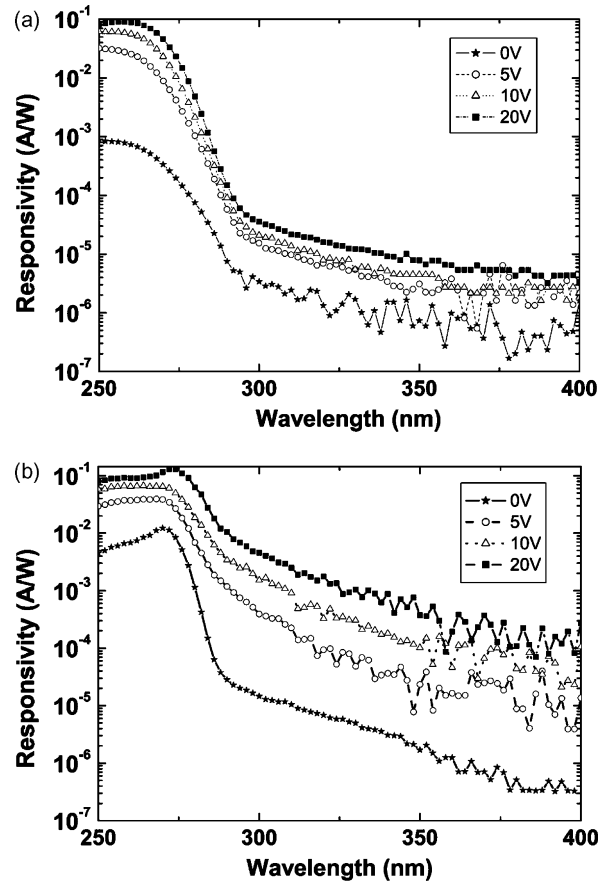


Fig. 2. Responsivity of a 150 μm diameter photodiodes from wafer I (a) and wafer II (b), respectively.

at zero bias, R_0 the zero volt dark impedance and A is the detector area, D^* is found as $4.68 \times 10^{13} \text{ cmHz}^{1/2} \text{ W}^{-1}$ and $D^* = 1.4 \times 10^{14} \text{ cmHz}^{1/2} \text{ W}^{-1}$ for the wafers I and II, respectively. The last figure corresponds to the highest detectivity value reported for an AlGaIn-based Schottky photodiodes.

From the photocurrent and dark current data, we calculated the avalanche gain by first taking the difference between the multiplied photocurrent and dark current data, and then normalizing it with respect to the unmultiplied difference of the photocurrent and dark current (Fig. 3). The maximum reproducible avalanche gain was 25 at 72 V reverse bias for the wafer I and 820 at 67 V for the wafer II under illumination at 280 nm wavelength with 20 μW optical power and the mono-chromator slith with is 2000 μm . The maximum E-fields at 67 V reverse bias are 0.5 and 1.67 MV/cm for wafers I and II, respectively. We proved reproducibility by way of taking the dark current measurement after several (10 scans) photocurrent measurements, in which we saw no significant change in dark current (Fig. 3),

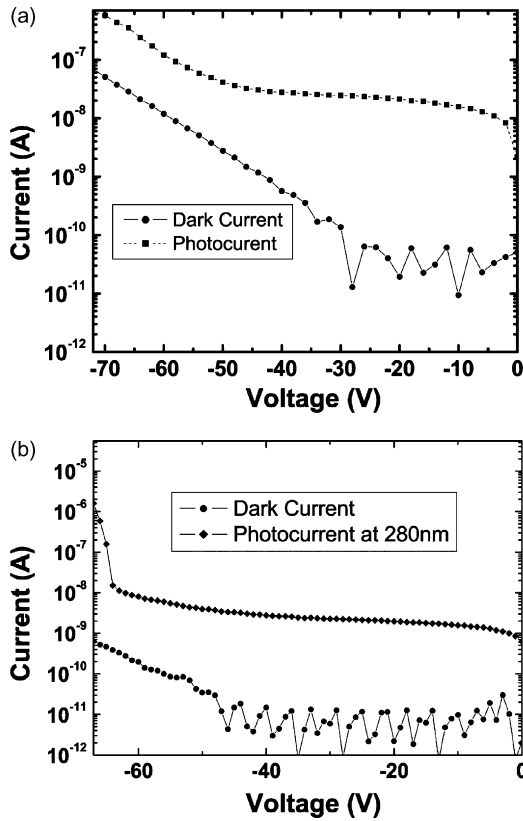


Fig. 3. Photocurrent and dark current measurements for wafers I and II at 280 nm wavelength.

and consequently, also none in the avalanche gain results (Fig. 4). In Fig. 3 we present the experimental data for the 10th scan.

To be sure about the unity gain voltage, we made the C–V measurement by LCR meter setup. We use a 30 μm diameter device in C–V measurements and as it can be seen from Fig. 5, the capacitance does not change after 20 V which is a sign that the device is fully depleted and does not absorb more light. We also understand this by measuring the photocurrent with a lock-in amplifier and a mono-chromator set-up. We check the photocurrent with varying voltages under 280 nm illumination with optical power intensity of 20 nW and the monochromator slith with is 500 μm. The photocurrent does not change much around 20 V as it can be seen in Fig. 6.

In summary, we present the MOCVD growth, fabrication, and characterization of AlGaIn-based solar-blind APDs. We improved the device performance by changing the wafer structure. The major change was to decrease the active layer thickness so that the defect density is lower. The second design was better than the first design in terms of dark current, breakdown voltage, detectivity, avalanche gain but it has lower UV–vis

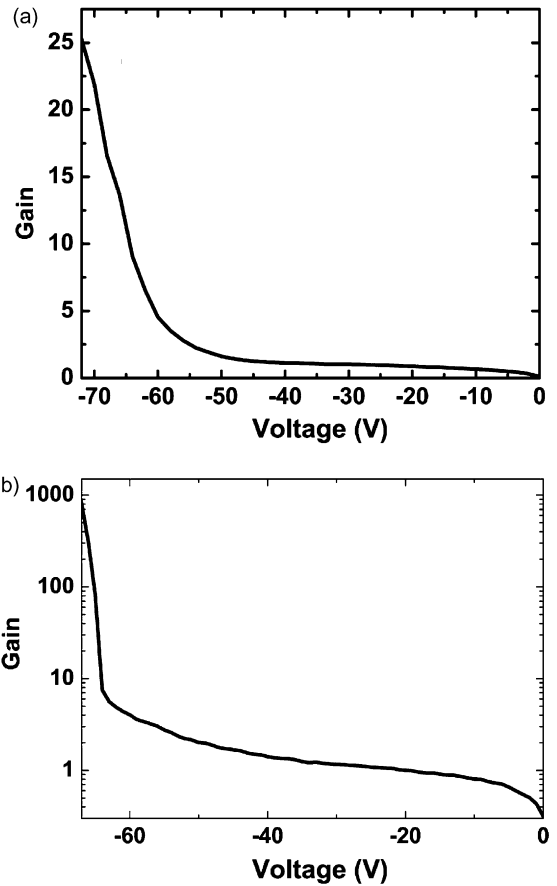


Fig. 4. Gain measurement data extracted from the photomultiplication results. Data taken from wafer I (a) and (b) wafer II.

rejection ratio. The gain in the active region of the devices is attributed to the avalanche multiplication of the photo-generated carriers. In later designs, we will try to improve the rejection ratio performance.

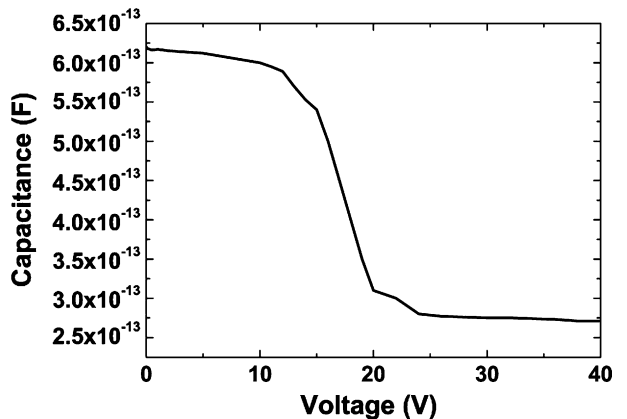


Fig. 5. C–V measurement from a 30 μm diameter device at 1 MHz frequency, and $V_{pp} = 50$ mV.

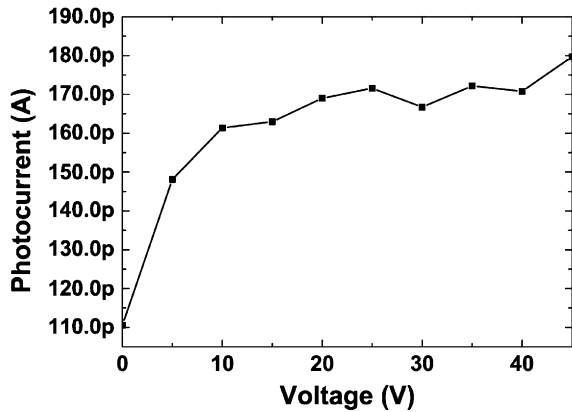


Fig. 6. Photocurrent from a large area device taken with a lock-in amplifier setup under low intensity illumination.

Acknowledgements

This work is supported by the European Union under the projects EU-NoE-METAMORPHOSE, EU-NoE-PHOREMOST, and TUBITAK under Projects Nos. 104E090, 105E066, 105A005, and 106A017. One of the authors (E.O.) also acknowledges partial support from the Turkish Academy of Sciences.

References

- [1] E. Ozbay, N. Biyikli, I. Kimukin, T. Tut, T. Kartaloglu, O. Aytur, *IEEE J. Sel. Top. Quant. Electron.* 10 (4) (2004) 742.
- [2] C.J. Collins, U. Chowdhury, M.M. Wong, B. Yang, A.L. Beck, R.D. Dupuis, *Electron. Lett.* 38 (2002) 824.
- [3] N. Biyikli, T. Kartaloglu, O. Aytur, I. Kimukin, E. Ozbay, *Appl. Phys. Lett.* 79 (2001) 2838.
- [4] N. Biyikli, I. Kimukin, T. Tut, O. Aytur, E. Ozbay, *Appl. Phys. Lett.* 81 (2002) 3272.
- [5] S. Butun, M. Gokkavas, Yu HongBo, E. Ozbay, *Appl. Phys. Lett.* 89 (2006) 073503.
- [6] J.C. Campbell, S. Demiguel, F. Ma, A. Beck, X. Guo, S. Wang, X. Zheng, X. Li, J.D. Beck, M.A. Kinch, A. Huntington, L.A. Coldren, J. Decobert, N. Tschertpner, *IEEE J. Quant. Electron.* 10 (2004) 777.
- [7] T. Tut, S. Butun, B. Butun, M. Gokkavas, H.B. Yu, E. Ozbay, *Appl. Phys. Lett.* 87 (2005) 223502.
- [8] N. Biyikli, I. Kimukin, T. Kartaloglu, O. Aytur, E. Ozbay, *Phys. Status Solidi (C)* 7 (2003) 2314.
- [9] Y. Wang, K. Brennan, P. Ruden, *IEEE J. Quant. Electron.* 27 (1991) 232.
- [10] P. Ruden, S. Krishnankutty, *IEEE Trans. Electron. Devices* 46 (1999) 2348.
- [11] C. Sevik, C. Bulutay, *Appl. Phys. Lett.* 83 (2003) 1382.
- [12] K.A. McIntosh, R.J. Molnar, L.J. Mahoney, A. Lightfoot, M.W. Geis, K.M. Molvar, I. Melngailis, R.L. Aggarwal, W.D. Goodhue, S.S. Choi, D.L. Spears, S. Verghese, *Appl. Phys. Lett.* 75 (1999) 3485.
- [13] J.C. Carrano, D.J.H. Lambert, C.J. Eiting, C.J. Collins, T. Li, S. Wang, B. Yang, A.L. Beck, R.D. Dupuis, J.C. Campbell, *Appl. Phys. Lett.* 76 (2000) 924.
- [14] A. Osinsky, M.S. Shur, R. Gaska, Q. Chen, *Electron. Lett.* 34 (1998) 691.
- [15] S. Verghese, K.A. McIntosh, R.J. Molnar, L.J. Mahoney, R.L. Aggarwal, M.W. Geis, K.M. Molvar, E.K. Duerr, I. Melngailis, *IEEE Electron. Dev. Lett.* 48 (2001) 502.
- [16] K.A. McIntosh, R.J. Molnar, L.J. Mahoney, K.M. Molvar, N. Efremov, S. Verghese, *Appl. Phys. Lett.* 76 (2000) 3938.
- [17] B. Yang, T. Li, K. Heng, C. Collins, S. Wang, J.C. Carrano, R.D. Dupuis, J.C. Campbell, M.J. Schurman, I.T. Ferguson, *IEEE J. Quant. Electron.* 36 (2000) 1389.
- [18] J.B. Limb, D. Yoo, J.H. Ryou, W. Lee, S.C. Shen, R.D. Dupuis, M.L. Reed, C.J. Collins, M. Wraback, D. Hanser, E. Preble, N.M. Williams, K. Evans, *Appl. Phys. Lett.* 89 (2006) 011112.
- [19] R. McClintock, A. Yasan, K. Minder, P. Kung, M. Razeghi, *Appl. Phys. Lett.* 87 (2005) 241123.
- [20] T. Tut, M. Gokkavas, B. Butun, S. Butun, E. Ulker, E. Ozbay, *Appl. Phys. Lett.* 89 (2006) 183524.